Quantifying the Roles of Changing Albedo, Emissivity, and Energy Partitioning in the Impact of Irrigation on Atmospheric Heat Content

S. C. PRYOR AND R. C. SULLIVAN

Department of Earth and Atmospheric Sciences, Cornell University, Ithaca, New York

T. WRIGHT

Antorcha, LLC, Logan, Utah

(Manuscript received 14 October 2015, in final form 22 January 2016)

ABSTRACT

Introduction of irrigated agriculture changes the partitioning of the surface energy flux between sensible and latent heat (H vs LE) and alters the albedo α and emissivity ε. In the absence of changes in the radiation components of the surface energy balance, the change in the Bowen ratio due to irrigation typically suppresses the local air temperature T but increases the total near-surface atmospheric heat content (as measured using equivalent potential temperature θ_e). While the effect of irrigation on surface energy partitioning due to enhanced surface and subsurface water availability has long been acknowledged, the roles of associated changes in ε and α have received less attention, and the scales and magnitudes of these effects remain uncertain. A new methodology designed for application to in situ and remote sensing data is presented and used to demonstrate that the net impact of irrigation on T and θ_e is strongly dependent on the regional climate, land cover in surrounding areas, and the amount of irrigation in the upwind fetch. The results suggest that the impact of the radiative forcing terms on net available energy is not negligible and may amplify or offset the impact from changed energy partitioning on T and θ_e depending on the specific regional climate and land cover.

1. Introduction and motivation

Irrigation represents a substantial perturbation to the global hydrological cycle and delivers about 2600 km^3 of water to the global land surface each year (~2% of annual overland precipitation) (Sacks et al. 2009). It has been a growing part of U.S. agriculture for over 60 years and affects a substantial fraction of the country; the area of land under irrigation is projected to increase (Gollehon and Quinby 2006; Moore et al. 2015). Changes in land use and land cover, including adoption of irrigation, have been identified as important drivers of local and regional climate (Adegoke et al. 2007; Pielke et al. 2011) and an important source of uncertainty in climate change detection and attribution studies (Fall et al. 2010).

Adoption of irrigation changes three components of the surface energy balance equation

$$S \times (1 - \alpha) + R_{\mathrm{li}} - R_{\mathrm{lo}} = H + \mathrm{LE} + G, \qquad (1)$$

where S = incoming solar radiation, α = albedo, R_{li} = counterradiated longwave radiation from the atmosphere, R_{lo} = outgoing longwave radiation from the surface ($R_{\mathrm{lo}} = \varepsilon\sigma T_s^4$, where ε = emissivity, σ = Stefan Boltzmann's constant, and T_s = surface temperature), H = sensible heat transfer, LE = latent heat transfer, and G = ground heat transfer:

1) *Reflection of incoming solar radiation by the surface.* Typical α values for dark-colored wet rough soils lie in the range 0.05–0.10, those for crops are typically 0.15–0.25, and those for light-colored flat dry soil are frequently in the range 0.35–0.40 (Dobos 2006). Thus, α for irrigated crops can be 0.05–0.10 lower than for surrounding natural vegetation, bare rock, and dry soil (Dobos 2006; Evett 2000). However, there is tremendous variability in the α of different

Corresponding author address: S. C. Pryor, Department of Earth and Atmospheric Sciences, Bradfield Hall, Cornell University, Ithaca, NY 14853.
E-mail: sp2279@cornell.edu.

DOI: 10.1175/JAMC-D-15-0291.1

surface types, and the difference in α due to irrigation (even the sign) is a complex function of crop, soil properties (e.g., organic carbon content or texture), surface roughness, and moisture content (Cierniewski et al. 2014).

2) *Emissivity of the surface for longwave radiation.* The ε of most soils is 0.88–0.94, while that of vegetation is ~0.94–0.98. The emissivity of vegetated surfaces, therefore, usually exceeds that of rocks and exposed soil (Evett 2000; Geiger et al. 2009; Pielke et al. 2011), and the ε of soils increases rapidly with increasing soil moisture (Alex and Behari 1998; Rees 2001).
3) *Partitioning of land surface energy transfer between sensible and latent heat fluxes (H vs* LE*) and thus the Bowen ratio (H*/LE*) (Hargreaves and Allen 2003; Pielke et al. 2011).* The presence of irrigation generally increases LE and thus the specific humidity q but differentially affects air temperature T during the day and night. Daily maximum temperatures are generally reduced by the increase in both LE and surface thermal energy storage [the specific heat of water ($4190\,\mathrm{J\,kg^{-1}\,K^{-1}}$) is higher than that for dry soil ($420–2510\,\mathrm{J\,kg^{-1}\,K^{-1}}$) (Geiger et al. 2009)]. Conversely, nighttime temperatures are typically increased by release of energy during condensation/deposition of water, the action of water vapor as a greenhouse gas (increasing R_{li}), and release of thermal energy absorbed during the day (Adegoke et al. 2007).

However, uncertainty remains regarding the scales of the effect and relative importance of impacts on the atmospheric heat content resulting from changes in the partitioning of H and LE, versus those that derive from changed α and ε.

Air temperature T provides an incomplete representation of lower atmospheric energy content, so equivalent potential temperature θ_e, which accounts for the contributions to static energy from both air temperature and specific humidity, is also used here as a response variable (Davey et al. 2006):

$$\theta_e = T\left(\frac{1000}{P}\right)^{\mathrm{Rd/Cpd}} + \frac{L(T)}{\mathrm{Cpd}}q, \qquad (2)$$

where T = air temperature, P = pressure, Rd = specific gas constant for air, Cpd = specific heat for dry air, $L(T)$ = latent heat of vaporization [$f(T)$], and q = specific humidity.

We present a new methodology designed for application to in situ and remote sensing data in which paired stations that are differentially influenced by irrigation are used to quantify the impact of irrigation on α, ε, T, and θ_e. The methodology is illustrated using high-quality meteorological data from the Automated Surface Observing System (ASOS; Sun et al. 2005) and U.S. Climate Reference Networks (CRN; Diamond et al. 2013), and estimates of irrigation and surface α and ε from the Moderate Resolution Imaging Spectroradiometer (MODIS).

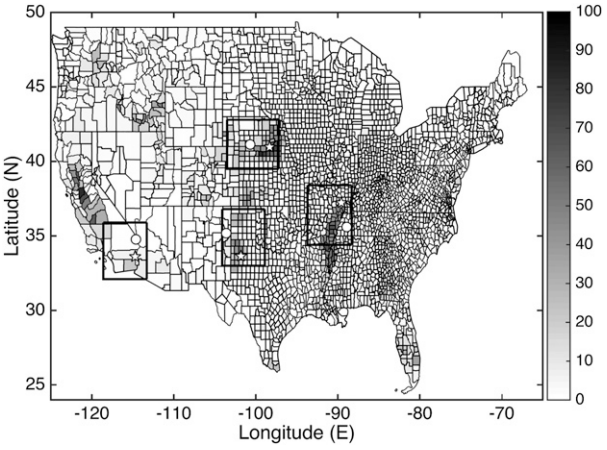

FIG. 1. USGS county-level irrigation (percentage of total land area) for 2010 based on data from http://waterdata.usgs.gov/nwis/wu. The boxes denote the four study regions. The irrigated and nonirrigated ASOS stations used herein are shown by the stars and circles, respectively.

2. Methods and data

An empirical methodology designed to quantify the theorized impacts of irrigation on changed land surface properties and the variability of changes in the energy balance components in space is illustrated using examples from four study regions: (i) California Mojave desert (CA), (ii) Mississippi River valley (MO), (iii) Nebraska central plains (NE), and (iv) Texas high plains (TX) (Fig. 1; Table 1). These regions represent some of the variation in climate, land surface characteristics, crop types and irrigation scales and mechanisms across the contiguous United States (Fig. 2).

For each ASOS station pair hourly measurements (1995–2014) of T are corrected to a common height above sea level (elevation of the lower measurement station) using a lapse rate of $6.5\,\mathrm{K\,km^{-1}}$ (T_{lap}), and θ_e is calculated from measured q, T, and P. Daily average S from measurements at CRN stations are assumed to be equal at each pair of stations within a region and are used in the analysis to estimate the impact of changing α on absorbed shortwave radiation [a key determinant of net radiation (NR), the left-hand side of Eq. (1)]. The quantity R_{lo} is not measured at ASOS or CRN stations so a first-order

TABLE 1. Monthly mean differences in air temperature dT (K), temperature adjusted for differences in station elevation dT_{lap} (K), and equivalent potential temperature $d\theta_e$ (K), based on data from the period 1995–2014. All differences are irrigated site − nonirrigated site. Data are shown by calendar month (rows) and study region (CA, MO, NE, and TX). Months for which a paired-sample *t* test leads to rejection of the null hypothesis that the mean difference T_{lap} and/or θ_e from the irrigated and nonirrigated site is equal to 0 at a significance level of 98% after the Bonferroni correction for the application of multiple tests (Simes 1986) is applied are shown in boldface type. Dominant crop types in the counties in which the meteorological stations are located are provided in the second row from the USDA 2014 National Agricultural Statistics Service report (http://www.nass.usda.gov/Charts_and_Maps/Crops_County/#db). Shown within the irrigated and nonirrigated stations blocks are their geographical location (lat and lon), elevation (m), and irrigation fetch Γ (s).

	CA			MO			NE			TX		
Dominant crop types	Alfalfa hay, durum wheat			Soybeans, corn; also cotton and rice			Corn, soybeans; also hay			Cotton, sorghum, and winter wheat		
Irrigated station	33.617°N, 114.717°W			37.233°N, 89.567°W			40.967°N, 98.317°W			33.650°N, 101.817°W		
	119			103			561			992		
	1866			2522			5239			2788		
Nonirrigated station	34.767°N, 114.617°W			35.600°N, 88.917°W			41.133°N, 100.683°W			35.183°N, 103.600°W		
	302			132			846			1237		
	77			74			1661			96		
Distance between stations (km)	130			190			200			236		
	dT (K)	dT_{lap} (K)	$d\theta_e$ (K)	dT (K)	dT_{lap} (K)	$d\theta_e$ (K)	dT (K)	dT_{lap} (K)	$d\theta_e$ (K)	dT (K)	dT_{lap} (K)	$d\theta_e$ (K)
Jan	0.36	**−0.83**	**−1.03**	2.75	**2.57**	**4.31**	0.05	**−1.81**	**−2.77**	1.25	**−0.34**	**−0.44**
Feb	0.38	**−0.80**	**−0.70**	2.36	**2.17**	**3.72**	0.36	**−1.49**	**−2.26**	1.34	**−0.25**	**−0.10**
Mar	0.31	**−0.88**	**−0.47**	2.00	**1.81**	**3.27**	0.59	**−1.26**	**−1.70**	1.40	**−0.19**	**1.33**
Apr	−0.18	**−1.37**	**−0.87**	1.45	**1.26**	**2.58**	1.46	**−0.39**	**−0.25**	1.67	0.08	**2.02**
May	−0.84	**−2.02**	**−1.08**	0.91	**0.73**	**2.20**	1.70	**−0.15**	**0.62**	1.24	**−0.35**	**3.70**
Jun	−1.36	**−2.55**	**−0.42**	0.31	**0.12**	**1.97**	1.53	**−0.32**	**0.76**	0.33	**−1.27**	**4.42**
Jul	−1.37	**−2.56**	**−0.22**	0.24	0.06	**1.50**	0.85	**−1.00**	**0.34**	0.02	**−1.57**	**0.56**
Aug	−0.84	**−2.03**	**0.38**	0.66	**0.47**	**1.81**	0.86	**−1.00**	**0.33**	0.58	**−1.02**	**1.10**
Sep	−0.40	**−1.59**	**1.33**	1.34	**1.15**	**3.29**	1.33	**−0.52**	**−0.03**	0.43	**−1.17**	**1.81**
Oct	−0.06	**−1.25**	**−0.43**	1.23	**1.04**	**3.18**	1.86	0.01	0.08	1.21	**−0.38**	**2.46**
Nov	0.15	**−1.04**	**−1.03**	1.46	**1.27**	**2.73**	1.72	−0.13	**−0.29**	1.25	**−0.34**	**0.98**
Dec	0.25	**−0.94**	**−1.24**	2.43	**2.24**	**3.87**	1.02	**−0.83**	**−1.34**	1.37	−0.22	**−0.37**
Annual	−0.30	−1.49	−0.49	1.43	1.24	2.87	1.11	−0.74	−0.54	1.01	−0.59	1.46

estimate of the change in R_{lo} due to the difference in emissivity $d\varepsilon$ is derived using Stefan–Boltzmann's law applied under the assumption that *T* measurements at 2 m are equal to the skin temperature T_s.

The influence of irrigation at a given station is a function of the time an upwind air parcel travels over irrigation. For each region one site defined as "irrigated" and one as "nonirrigated" were selected to make up a station pair. A site is defined as irrigated if >25% of land in either a 10- or 50-km radius in the prevailing upwind direction is irrigated. Conversely, a site is defined as nonirrigated if <15% of land in either a 10- or 50-km radius in the prevailing wind direction is irrigated. The overirrigation fetch time scale Γ is the equivalent mean number of seconds over irrigation:

$$\Gamma = \sum_{i=1}^{16}\left[\left(\frac{50\,000\,\text{m}}{||U_i||}\right)(I_i)(f_i)\right], \qquad (3)$$

where $||U_i||$ = mean wind speed at 10 m in one of 16 direction sectors *i* (m s^{-1}), f_i = frequency of winds in that sector, and I_i = fraction of area within 50 km of the station in that sector that is irrigated according to the MODIS Irrigated Agriculture Dataset. In this dataset, MODIS pixels with highest peak normalized difference vegetation index are sequentially classified as irrigated until the area of irrigation is approximately equal to that in U.S. Department of Agriculture (USDA) county-level statistics (Brown and Pervez 2014).

Station pairs are selected to maximize the difference in Γ, while seeking to maintain a reasonable separation distance to allow an implicit assumption of a similar base climate (Table 1). For each region, the stations that are defined as being influenced by irrigation have estimated Γ that exceeds those of the nonirrigated sites by at least a factor of 3 (Table 1).

MODIS visible (0.3–0.7 μm) white-sky albedo (MCD43A3) is generated every 16 days at 0.5-km resolution using surface reflectances at viewing angles from all 16 orbital paths (Schaaf et al. 2002; Taberner et al. 2010). The estimated α is likely accurate to within ±0.01–0.03 (Pinty et al. 2011). Emissivity estimates are based on irradiance in the infrared (band 31; 10.78–11.28 μm; MOD11A2). The

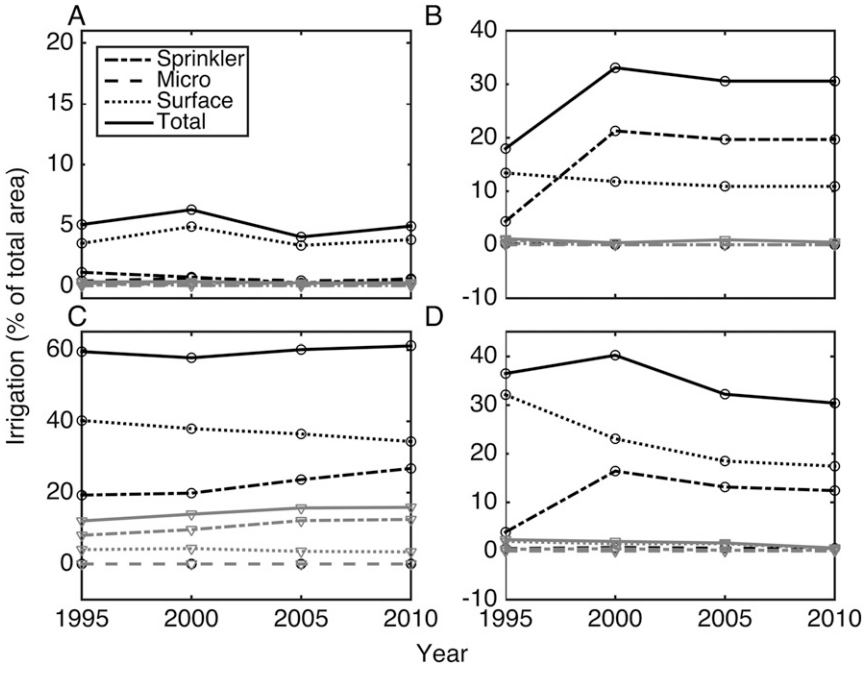

FIG. 2. Percentage of total area in the county containing the ASOS stations under irrigation (and by irrigation mechanism shown in legend) for (a) CA, (b) MO, (c) NE, and (d) TX. Black lines (circles) are the irrigated stations; gray lines (inverted triangles) are the nonirrigated stations. Locations of sites are given in Fig. 1. Data are from http://waterdata.usgs.gov/nwis/wu. Note the scales of the ordinate axes differ in each of the panels.

dataset includes 8-day ε estimates at 1 km (Hulley et al. 2012; Wan 2008) that are reported to have an accuracy of ± 0.015 (Hulley et al. 2012; Jacob et al. 2004). Herein, we use an average of all α and ε retrievals within 1 km of each ASOS station during June–August of 2000–14 to derive an average α and ε for the nonirrigated and irrigated sites and generate an average difference (dX; irrigated site − nonirrigated site) for those parameters (Table 2). Naturally, the representativeness of these estimates is a function of the number of cloud-free pixels, and, as discussed further below, the mean difference in these surface properties must be viewed with caution.

3. Results

Table 1 shows the monthly mean difference between paired air temperature measurements (both T, and those adjusted to a common elevation above sea level,

TABLE 2. Summary of data for June–August 2000–14 in each region. Note all difference values are irrigated site − nonirrigated site. T = mean June–August temperature (K) of the paired sites, S = daily mean measured incoming solar radiation (W m^{-2}), R_{lo} = daily mean outgoing longwave radiation (W m^{-2}) calculated under the assumption that the air temperature measured at 2 m is equal to the skin temperature (T_s); α = mean summer albedo at the nonirrigated site, dα = difference in albedo, and dFα = difference in net radiation due to the difference in albedo (note positive values indicate increased NR); ε = mean emissivity (nonirrigated site), dε = difference in emissivity, and dFε= difference in net radiation due to the difference in emissivity (W m^{-2}); dF = total difference in net radiation due to the differences in both albedo and emissivity (W m^{-2}); dT$_s$ is an approximation of the response of skin temperature (K) to the difference in NR, computed using the mean T and ε from the nonirrigated site. The final two columns show dT$_{lap}$ = difference in observed air temperature (June–August 2000–14) corrected to a common elevation (K), and dθ_{eobs} = difference in equivalent potential temperature (K).

	Mean values			Mean α and ε, difference in paired stations, radiative forcing, and thermal response								Observations	
Region	T (K)	S (W m^{-2})	R_{lo} (W m^{-2})	α	dα (10^{-2})	dFα (W m^{-2})	ε	dε (10^{-3})	dFε (W m^{-2})	dF (W m^{-2})	dT$_s$ (K)	dT$_{lap}$ (K)	dθ_{eobs} (K)
CA	308.3	308	498	0.12	−3.05	9.40	0.97	−0.28	0.14	9.54	1.35	−2.52	−0.32
MO	298.4	254	441	0.06	−0.70	1.78	0.98	0.44	−0.19	1.58	0.19	0.21	1.77
NE	296.1	255	427	0.07	−0.77	1.96	0.98	0.01	−0.004	1.96	0.44	−0.78	0.53
TX	299.4	280	448	0.11	−0.31	0.87	0.98	2.34	−1.05	−0.18	−0.28	−1.15	2.31

T_{lap}) and equivalent potential temperature θ_e at stations close to irrigation versus stations not affected by irrigation. According to a paired-sample t test, the hypothesis that the mean difference is equal to 0 is rejected at a 98% confidence level for virtually all calendar months for each of the paired stations (Table 1). As expected, the differences in T_{lap} and θ_e at irrigated versus nonirrigated sites are generally (though not uniformly) of largest magnitude during the growing season, when S and irrigation use are highest. For this reason the attribution analyses presented below focus on the climatological summer months (June–August), although it must be acknowledged that the growing and crop peak water demand seasons for some of the crops prevalent in the study regions extend greatly beyond these calendar months (Döll and Siebert 2002; Steduto et al. 2012).

In the paired samples from CA, NE, and TX, T_{lap} is uniformly lower at the irrigated sites. The mean monthly dT_{lap} is about −1.5 K in the paired sample from CA. Estimates for the growing season indicate larger impacts, with mean dT_{lap} from −2 to −3 K. Mean dT_{lap} from TX and NE are from approximately −0.5 to −0.8 K and thus are of lower magnitude than the data from CA. But, like the CA paired sites, the irrigation-impacted stations in NE and TX exhibit lower T_{lap} in virtually all calendar months (Table 1). Results for the paired stations in MO indicate slightly higher T_{lap} at the irrigated station, possibly because of a difference in the base climate of the stations, but dT_{lap} is smallest in the summer, consistent with cooling due to irrigation. Results for this station pair emphasize the difficulty in quantifying the impact of irrigation on local to regional climates and illustrate an important confounding factor—the potential for upstream regional-scale irrigation to affect the nonirrigated sites. The area of irrigated land in the prevailing winds during the growing season in NE and MO are far greater than either TX or CA (Fig. 1), potentially meaning that sites considered herein as nonirrigated may be contaminated by irrigation more than 50 km upstream.

The higher LE and resulting increase in q due to irrigation is manifest as higher θ_e at the irrigated sites during the growing season in MO, NE, and TX ($d\theta_e$ during June–August ranges from 0.3 to 4.4 K). A priori expectations were that the lower q and larger regional vapor pressure deficits (Gaffen and Ross 1999) in CA would cause a greater impact of irrigation on LE and therefore θ_e. However, although $d\theta_e$ is generally less negative than dT_{lap}, $d\theta_e$ for the CA paired stations is generally negative (indicating the nonirrigated site has higher θ_e) (Table 1). A partial explanation for this finding may be that Γ for the CA irrigation-impacted site is smaller than in the other three regions (Table 1). However, it may also reflect compensating forcing deriving from modification of albedo and/or emissivity (see below).

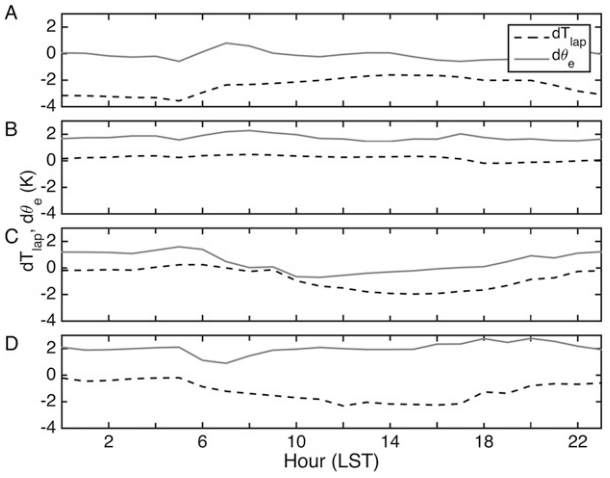

FIG. 3. Hourly mean difference in summer (June−August 1995–2014) air temperature corrected for difference in site elevation (dT_{lap}) and equivalent potential temperature ($d\theta_e$) between irrigated and nonirrigated stations in (a) CA, (b) MO, (c) NE, and (d) TX. Note that all times are expressed in local standard time (LST). The sites are located in the central time zone except for those in (a), which are in the Pacific time zone.

In addition to the clear seasonality in dT and $d\theta_e$ (Table 1), these variables also exhibit diurnal signatures (Fig. 3). The quantity $d\theta_e$ is of very small magnitude or positive in all hours of the day, whereas dT_{lap} in MO, NE, and TX is, as expected, most negative during the afternoon. CA is an exception in that dT_{lap} is negative throughout the day but of smallest magnitude during the afternoon. This may be due to confounding influences such as changes in α and/or ε or in the timing, extent, or type of irrigation (surface flooding vs sprinkler; Fig. 2).

In all regions mean summertime α at both the irrigated and nonirrigated sites is relatively low (0.05–0.13; Table 2). In accord with our expectations, the presence of irrigation is generally associated with lower α (Table 2). Using S from the nearest CRN stations and the difference in mean α at the irrigated versus nonirrigated sites, an estimate for the resulting increase in available NR is obtained. For CA this calculation results in considerably higher NR (9.4 W m^{-2}) at the irrigated station, while in the other regions the impact is more modest (NR increased by up to 2 W m^{-2}). This change in α thus acts as a positive forcing on T, that is largest at the CA paired stations where $d\alpha$ is about 20% of the nonirrigated site mean summertime α (Table 2). In CA, MO and NE the impact of $d\varepsilon$ on NR is smaller than that deriving from $d\alpha$ (from −0.19 to +0.14 W m^{-2}), while in TX it is of comparable magnitude. The combined impact of the difference in α and ε on NR is strongly positive in

CA, and weakly positive in MO and NE leading to enhanced surface energy availability and thus higher "predicted" air temperatures (by 0.2–1.5 K; Table 2). Conversely, in TX the combined effect of $d\alpha$ and $d\varepsilon$ is to slightly reduce NR and thus predicted T_{lap} at the irrigated site.

4. Discussion

The purpose of this article is to highlight the need for deeper understanding the total impact of irrigation on climate change at the regional scale, and specifically for the need to include the impacts on parameters relating to shortwave and longwave radiation. We further seek to propose an approach that maybe applied to empirically quantify the impact of irrigation on the different terms in the energy balance in different climate regions. The results of our limited proof of principle must be considered only *very approximate* estimates of the possible thermal response to changes in NR due to the assumptions applied in their generation (e.g., that the 2-m air temperature is equal to the skin temperature) and the high uncertainty in $d\alpha$ and $d\varepsilon$. However, the results shown in Table 2 imply that irrigation may substantially alter NR in some regions and may act to greatly confound interpretation of T and θ_e time series in regions with substantial irrigation. Observations indicate summer air temperatures are lower (on average) at sites impacted by irrigation in CA, NE, and TX (by 0.78–2.4 K). Thus it appears that the change in flux partitioning dominates the net impact on air temperatures in these regions. However, the impacts of changes in α and ε due to irrigation in CA, MO, and NE generally act to offset some fraction of the cooling of air temperatures due to changes in the surface energy partitioning. For example, the observed summertime dT_{lap} is -2.5 K in CA, while the NR forcing is estimated to result in dT_s of nearly $+1.4$ K. Thus it may be that changes in surface properties are masking up to one-third of the cooling due to enhanced water availability. However, the magnitude of these effects is regionally specific, and indeed the impact of $d\alpha$ and $d\varepsilon$ on NR is of the opposite sign in TX and indicates the change in surface properties may enhance surface cooling in some regions. A comprehensive analysis of region-to-region variations in the magnitude of the irrigation-induced changes in the components of the surface energy balance would have high scientific value. However, there are a number of challenges to such a meta-analysis, including 1) the limited availability of paired sites with similar base climates, elevation, and cropping that have long, complete time series derived from identical instrumentation but different fetch characteristics in terms of irrigation coverage, and 2) the uncertainty associated with the remote sensing estimates of surface properties [see further details below, and prior discussions regarding data needs for land surface–atmosphere coupling studies (Sellers et al. 1995)]. It should also be acknowledged that both California and Texas have experienced severe, long-lasting droughts during the study period, and in recent years both Missouri and Nebraska have experienced a number of growing seasons with above-average precipitation (Lehmann and Coumou 2015; Shukla et al. 2015; Trepanier et al. 2015). Year-to-year variations in crop selection (or the relative fraction of area under the dominant crops shown in Table 1) and in precipitation receipt may have greatly influenced the amount of water used in irrigation in individual years within individual counties. Such effects are difficult to quantify with the once-every-5-yr county-level irrigation data available from the USDA and therefore are neglected in the current analysis.

It is important to acknowledge that the methodology proposed herein is subject to a range of caveats and uncertainties, and that further research is necessary to test the generalizability of our findings and to refine the technique to increase the signal-to-noise ratio. The correction of the air temperature time series to a common altitude introduces potential errors in the dT_{lap} and $d\theta_e$ estimates. Further, the differences in α and ε at the irrigated versus nonirrigated sites are of very small magnitude and therefore are difficult to detect using currently available remote sensing measurements. Satellite-derived global surface albedo products are of high value to studies such as that presented herein and are being increasingly well quantified. However, they are subject to uncertainties including those challenges inherent in the measurement (e.g., reradiation of the earth's surfaces is not Lambert distributed, and atmospheric attenuation) and related to ground truthing (including spatial scaling errors between satellite and field measurements; Mira et al. 2015). Further, α is a function of irradiance conditions and thus varies as a function of hour of the day in a way that differs between soil and crops (Kimes et al. 1987), while the MODIS satellite overpasses only once per day. Despite these important caveats that pertain to the currently available data, the approach we propose may be useful in deconvoluting the impact of irrigation on surface properties and energy exchange, providing observational constraints on numerical attribution studies of the atmospheric impacts of irrigation, and can be readily applied in other regions or to other datasets. For example, it could be applied to higher-resolution (and higher

accuracy) remote sensing data as they become available or to meteorological data from mesonets to examine station pairs that are less separated geographically and thus are less vulnerable to variations in base climate.

Acknowledgments. We acknowledge grants to SCP from NSF (1339629 and 1502400) to RCS from NASA (14-EARTH14F-0207); useful conversations with R. J. Barthelmie, G. Olyphant, and J. T. Schoof; and the many scientists who developed the data sets used herein. The comments of three reviewers improved the quality and clarity of this manuscript.

REFERENCES

Adegoke, J. O., R. Pielke, and A. M. Carleton, 2007: Observational and modeling studies of the impacts of agriculture-related land use change on planetary boundary layer processes in the central US. *Agric. For. Meteor.*, **142**, 203–215, doi:10.1016/j.agrformet.2006.07.013.

Alex, Z. C., and J. Behari, 1998: Laboratory evaluation of emissivity of soils. *Int. J. Remote Sens.*, **19**, 1335–1340, doi:10.1080/014311698215478.

Brown, J. F., and M. S. Pervez, 2014: Merging remote sensing data and national agricultural statistics to model change in irrigated agriculture. *Agric. Syst.*, **127**, 28–40, doi:10.1016/j.agsy.2014.01.004.

Cierniewski, J., A. Karnieli, C. Kaźmierowski, and J. Ceglarek, 2014: A tool for predicting diurnal soil albedo variation in Poland and Israel. *EARSeL eProc.*, **13**, 36–40, doi:10.12760/02-2014-1-07.

Davey, C. A., R. A. Pielke Sr., and K. P. Gallo, 2006: Differences between near-surface equivalent temperature and temperature trends for the eastern United States: Equivalent temperature as an alternative measure of heat content. *Global Planet. Change*, **54**, 19–32, doi:10.1016/j.gloplacha.2005.11.002.

Diamond, H. J., and Coauthors, 2013: U.S. Climate Reference Network after one decade of operations status and assessment. *Bull. Amer. Meteor. Soc.*, **94**, 485–498, doi:10.1175/BAMS-D-12-00170.1.

Dobos, E., 2006: Albedo. *Encyclopedia of Soil Science*, R. Lal, Ed., CRC Press, 64–66.

Döll, P., and S. Siebert, 2002: Global modeling of irrigation water requirements. *Water Resour. Res.*, **38**, doi:10.1029/2001WR000355.

Evett, S. R., 2000: Energy and water balances at soil–plant–atmosphere interfaces. *Handbook of Soil Science*, M. E. Sumner, Ed., CRC Press, A129–A182.

Fall, S., D. Niyogi, A. Gluhovsky, R. A. Pielke, E. Kalnay, and G. Rochon, 2010: Impacts of land use land cover on temperature trends over the continental United States: Assessment using the North American Regional Reanalysis. *Int. J. Climatol.*, **30**, 1980–1993, doi:10.1002/joc.1996.

Gaffen, D. J., and R. J. Ross, 1999: Climatology and trends of U.S. surface humidity and temperature. *J. Climate*, **12**, 811–828, doi:10.1175/1520-0442(1999)012<0811:CATOUS>2.0.CO;2.

Geiger, R., R. H. Aron, and P. Todhunter, 2009: *The Climate near the Ground.* Rowman and Littlefield, 584 pp.

Gollehon, N., and W. Quinby, 2006: Irrigation resources and water costs. *Agricultural Resources and Environmental Indicators*, Economic Research Service/USDA, 24–32.

Hargreaves, G. H., and R. G. Allen, 2003: History and evaluation of Hargreaves evapotranspiration equation. *J. Irrig. Drain. Eng.*, **129**, 53–63, doi:10.1061/(ASCE)0733-9437(2003)129:1(53).

Hulley, G., S. Hook, and C. Hughes, 2012: MODIS MOD21 land surface temperature and emissivity Algorithm Theoretical Basis Document. Jet Propulsion Laboratory, California Institute of Technology, JPL Publ. 12–17, 102 pp. [Available online at http://emissivity.jpl.nasa.gov/downloads/examples/documents/MOD21_LSTE_ATBD_Hulley_v2.0_20121116_pmbv1.pdf.]

Jacob, F., F. Petitcolin, T. Schmugge, E. Vermote, A. French, and K. Ogawa, 2004: Comparison of land surface emissivity and radiometric temperature derived from MODIS and ASTER sensors. *Remote Sens. Environ.*, **90**, 137–152, doi:10.1016/j.rse.2003.11.015.

Kimes, D. S., P. J. Sellers, and W. W. Newcomb, 1987: Hemispherical reflectance variations of vegetation canopies and implications for global and regional energy budget studies. *J. Climate Appl. Meteor.*, **26**, 959–972, doi:10.1175/1520-0450(1987)026<0959:HRVOVC>2.0.CO;2.

Lehmann, J., and D. Coumou, 2015: The influence of mid-latitude storm tracks on hot, cold, dry and wet extremes. *Sci. Rep.*, **5**, 17491, doi:10.1038/srep17491.

Mira, M., M. Weiss, F. Baret, D. Courault, O. Hagolle, B. Gallego-Elvira, and A. Olioso, 2015: The MODIS (collection V006) BRDF/albedo product MCD43D: Temporal course evaluated over agricultural landscape. *Remote Sens. Environ.*, **170**, 216–228, doi:10.1016/j.rse.2015.09.021.

Moore, B., A. Coleman, M. Wigmosta, R. Skaggs, and E. Venteris, 2015: A high spatiotemporal assessment of consumptive water use and water scarcity in the conterminous United States. *Water Resour. Manage.*, **29**, 5185–5200, doi:10.1007/s11269-015-1112-x.

Pielke, R. A., Sr., and Coauthors, 2011: Land use/land cover changes and climate: Modeling analysis and observational evidence. *Wiley Interdiscip. Rev.: Climate Change*, **2**, 828–850, doi:10.1002/wcc.144.

Pinty, B., M. Taberner, V. R. Haemmerle, S. R. Paradise, E. Vermote, M. M. Verstraete, N. Gobron, and J.-L. Widlowski, 2011: Global-scale comparison of MISR and MODIS land surface albedos. *J. Climate*, **24**, 732–749, doi:10.1175/2010JCLI3709.1.

Rees, W. G., 2001: *Physical Principles of Remote Sensing*. 2nd ed. Cambridge University Press, 343 pp.

Sacks, W. J., B. I. Cook, N. Buenning, S. Levis, and J. H. Helkowski, 2009: Effects of global irrigation on the near-surface climate. *Climate Dyn.*, **33**, 159–175, doi:10.1007/s00382-008-0445-z.

Schaaf, C. B., and Coauthors, 2002: First operational BRDF, albedo nadir reflectance products from MODIS. *Remote Sens. Environ.*, **83**, 135–148, doi:10.1016/S0034-4257(02)00091-3.

Sellers, P., and Coauthors, 1995: Remote sensing of the land surface for studies of global change: Models—algorithms—experiments. *Remote Sens. Environ.*, **51**, 3–26, doi:10.1016/0034-4257(94)00061-Q.

Shukla, S., A. Steinemann, S. F. Iacobellis, and D. R. Cayan, 2015: Annual drought in California: Association with monthly precipitation and climate phases. *J. Appl. Meteor. Climatol.*, **54**, 2273–2281, doi:10.1175/JAMC-D-15-0167.1.

Simes, R. J., 1986: An improved Bonferroni procedure for multiple tests of significance. *Biometrika*, **73**, 751–754, doi:10.1093/biomet/73.3.751.

Steduto, P., T. C. Hsiao, D. Raes, and E. Fereres, 2012: Crop yield response to water. Food and Agriculture Organization of the United Nations, 505 pp. [Available online at http://www.fao.org/docrep/016/i2800e/i2800e.pdf.]

Sun, B. M., C. B. Baker, T. R. Karl, and M. D. Gifford, 2005: A comparative study of ASOS and USCRN temperature measurements. *J. Atmos. Oceanic Technol.*, **22**, 679–686, doi:10.1175/JTECH1752.1.

Taberner, M., B. Pinty, Y. Govaerts, S. Liang, M. Verstraete, N. Gobron, and J. L. Widlowski, 2010: Comparison of MISR and MODIS land surface albedos: Methodology. *J. Geophys. Res.*, **115**, D05101, doi:10.1029/2009JD012665.

Trepanier, J. C., M. J. Roberts, and B. D. Keim, 2015: Trends and spatial variability in dry spells across the south-central United States. *J. Appl. Meteor. Climatol.*, **54**, 2261–2272, doi:10.1175/JAMC-D-14-0319.1.

Wan, Z., 2008: New refinements and validation of the MODIS land-surface temperature/emissivity products. *Remote Sens. Environ.*, **112**, 59–74, doi:10.1016/j.rse.2006.06.026.